coatings

MDPI

Article

Preparation of Alumina Thin Films by Reactive Modulated Pulsed Power Magnetron Sputtering with Millisecond Pulses

Alexander V. Tumarkin [1], Dobrynya V. Kolodko [1,2], Maksim M. Kharkov [1], Tatiana V. Stepanova [1], Andrey V. Kaziev [1], Nikolay N. Samotaev [1,*] and Konstantin Yu. Oblov [1]

[1] Moscow Engineering Physics Institute, National Research Nuclear University MEPhI, 115409 Moscow, Russia; avkaziev@mephi.ru (A.V.K.)
[2] Kotelnikov Institute of Radioengineering and Electronics RAS, Fryazino Branch, 141190 Fryazino, Russia
* Correspondence: nnsamotaev@mephi.ru

Abstract: This paper aims to investigate the quality of thin alumina films deposited on glass samples using magnetron sputtering in the reactive modulated pulsed power mode (MPPMS) and evaluate the process productivity. The aluminum target was sputtered in Ar/O_2 gas mixtures with different fractions of oxygen in the total gas flow, in the fixed pulsed voltage mode. The pulse-on duration was varied between 5 and 10 ms, while the pulse-off time was 100 or 200 ms. The dependences of mass deposition rate and discharge current on the oxygen flow were measured, and the specific deposition rate values were calculated. Prepared coatings had a thicknesses of 100–400 nm. Their quality was assessed by scratch testing and by measuring density, refractory index, and extinction coefficient for different power management strategies. The strong influence of pulse parameters on the coating properties was observed, resulting in a maximum density of 3.6 g/cm^3 and a refractive index of 1.68 for deposition modes with higher duty cycle values. Therefore, adjusting the pulse-on and pulse-off periods in MPPMS can be used not only to optimize the deposition rate but also as a tool to tune the optical characteristics of the films. The performance of the studied deposition method was evaluated by comparing the specific growth rates of alumina coatings with the relevant data for other magnetron discharge modes. In MPPMS, a specific deposition rate of 200 nm/min/kW was obtained for highly transparent Al_2O_3, without using any dedicated feedback loop system for oxygen pressure stabilization, which makes MPPMS superior to short-pulse high-power impulse magnetron sputtering (HiPIMS) modes.

Keywords: magnetron sputtering; reactive sputtering; alumina thin films; MPPMS; HiPIMS

Citation: Tumarkin, A.V.; Kolodko, D.V.; Kharkov, M.M.; Stepanova, T.V.; Kaziev, A.V.; Samotaev, N.N.; Oblov, K.Y. Preparation of Alumina Thin Films by Reactive Modulated Pulsed Power Magnetron Sputtering with Millisecond Pulses. *Coatings* **2024**, *14*, 82. https://doi.org/10.3390/coatings14010082

Academic Editor: Choongik Kim

Received: 19 December 2023
Revised: 31 December 2023
Accepted: 5 January 2024
Published: 7 January 2024

1. Introduction

Preparation of thin-film coatings is a crucial process for many production steps in electronics, optical instrumentation, machining. Specifically, oxide coatings are widely applied in these areas because of their unique combinations of electrical and mechanical properties. In optical applications, coatings based on oxides of various metals are most in demand since they have high refractive indices and good transparency. For example, interference coatings are used to obtain high reflectance (mirror coatings), to change the polarization of radiation (interference polarizers), and also to increase transmittance and contrast (antireflection coatings) [1–3]. In electronics, metal oxide films are frequently used as insulating layers and interfaces for matching adjacent materials' thermal expansion coefficients [4,5]. They are also valuable for creating durable electronic components because of their ability to withstand high temperatures and harsh environments [6–11]. Among metal oxide coatings applied in these fields, Al_2O_3 (alumina) is widely presented [12].

There are several well-developed methods for applying such thin-film coatings, which nevertheless have certain application limitations. For example, chemical vapor deposition (CVD) requires a high substrate temperature [13] and does not allow precise control of

the thickness of the resulting coating. One of the most widely applied physical vapor deposition (PVD) methods—cathodic arc evaporation—cannot fully guarantee the absence of microscale inclusions and associated defects in the deposited film [14]. Another popular PVD method for producing metal oxide coatings is reactive magnetron sputtering, which is realized when a magnetron discharge is formed in a mixture of argon with the addition of oxygen.

Magnetron sputtering (MS) systems vary largely in the power application approach, and apart from the most popular direct current (DC), mid-frequency (MF, or pulsed DC), and radiofrequency (RF) modes, currently we have a choice of more sophisticated impulse discharge regimes, such as high-power impulse magnetron sputtering (HiPIMS), modulated pulsed power magnetron sputtering (MPPMS), deep oscillation magnetron sputtering (DOMS), and their combinations.

When operating in a reactive gas environment, classical MS modes (DC and RF) exhibit specific technological difficulties [15–17], such as target surface arcing, disappearing anode effect, and low plasma density near the substrate (for the DC case), and low deposition rate, low efficiency, and limited scaling opportunity (for the RF case). Also, one of the most prominent features of reactive sputtering is strong nonlinear hysteresis coupling between reactive gas flow, discharge characteristics, and deposition rate [18,19], which requires advanced process control techniques for maintaining deposition stability and reproducibility.

The use of impulse modes (HiPIMS, MPPMS, DOMS), in many cases, allows the mitigation of the complications of reactive sputtering associated with poisoning of the target and anode surfaces with non-conductive compounds [20–26]. HiPIMS is capable of obtaining plasmas with a high ionization degree by using short (30–150 μs) pulses with peak power density levels of 1–10 kW/cm^2. The distinct feature of MPPMS is a longer (1–10 ms-scale) pulse, while the degree of ionization in MPPMS is comparable to that in HiPIMS [27]. Enhanced fluxes of ions facilitate the growth of coatings with high density, which is relevant for applications in electronics, optics, and the production of tools. However, the productivity of pulsed processes is usually lower than that of conventional ones.

In [28], HiPIMS and DC MS are compared by their performance of depositing Al_2O_3 films by sputtering an aluminum target in a mixture of argon and oxygen using the HiPIMS and DC MS methods. The experiment was conducted in Ar/O_2 at a total pressure of 0.8 Pa. The average power in HiPIMS modes was 60% higher than in DC to compensate for the lower deposition rate. When using DC, a sharp decrease in the deposition rate was observed after a particular critical value of oxygen flow, which is associated with target poisoning. In the case of HiPIMS, the deposition rate decreased more smoothly than in DC, and no hysteresis was observed. It was concluded that the tradeoff between coating quality and deposition rate is achieved in this transition region. Hence, the use of HiPIMS provides more consistent performance during oxide deposition.

In [29], a comparative analysis is performed for the optical properties of Al_2O_3 films obtained by HiPIMS and DC MS. Diagnostics of the samples was carried out using spectral ellipsometry. The refractive index values for films obtained by different methods and under different conditions vary significantly, and the authors draw the following conclusions: (1) the refractive index for samples obtained using the HiPIMS method increases with increasing magnetron discharge power; (2) samples obtained by DC MS exhibit an increase in refractive index with decreasing deposition rate, as well as with increasing substrate temperature; and (3) the refractive index for samples obtained by annealing is comparable to the refractive index of a sample deposited by magnetron sputtering and at a substrate temperature of 500 °C. It should be noted that the maximum refractive index among the samples obtained without additional substrate heating corresponds to the HiPIMS method (n = 1.60).

Despite improvements in reactive sputtering stability in HiPIMS as compared to DC MS, the deposition rate of oxides is comparatively low. In pursuit of increasing the growth

rate of compound coatings without compromising their quality, the combinations of HiPIMS+MF modes were considered [24,30–32], and MPPMS modes were developed, which combine high ionization degree of the deposition flux and high deposition rates [33–35]. The application of MPPMS modes showed good performance for metallic and nitride coating deposition. For oxide coatings, DOMS mode, which is a modified version of MPPMS, is considered much more frequently. The application of DOMS mode together with closed-loop feedback control of oxygen partial pressure increases the productivity of Al_2O_3 coating preparation with respect to HiPIMS and allows the elimination of the arcing on the target [36].

The purpose of this work is to study the performance of Al_xO_y coatings deposition in MPPMS modes without any feedback control and without applying external substrate heating, and to compare it with typical HiPIMS data. The quality of alumina coatings is evaluated by their density, optical parameters, and adhesion to the substrate.

2. Experimental Methods

2.1. Experimental Setup

A scheme of the installation used for alumina films deposition is shown in Figure 1.

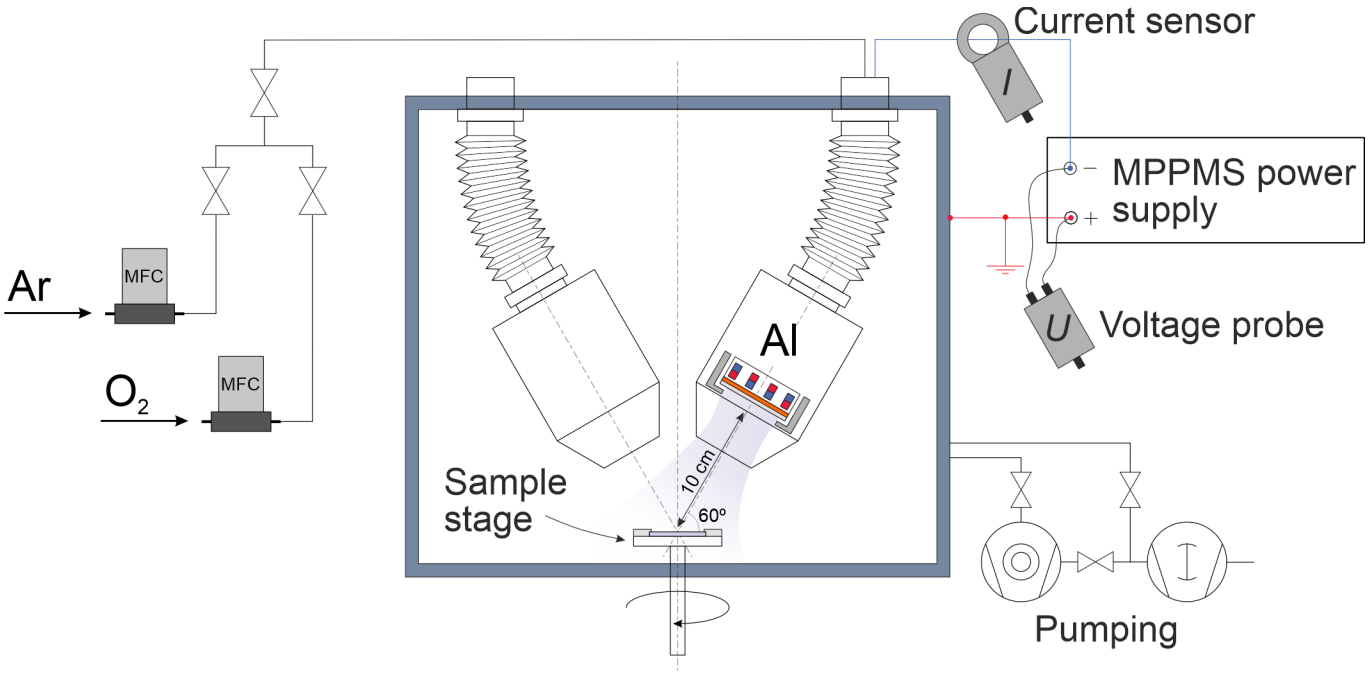

Figure 1. Setup of the magnetron sputtering system.

It is a confocal magnetron sputtering setup comprising slightly unbalanced circular magnetrons Magneto-3GABS (Pinch, LLC., Moscow, Russia). In the current experiments, a single magnetron was used out of three available in the installation. Sputtering was performed from a 76.2 mm-diameter aluminum target with 99.999% purity (Girmet, LLC., Moscow, Russia). The samples were placed at the bottom of the vacuum chamber, attached to a stage rotating at a frequency of 1.5 rpm. The distance between the magnetron cathode and the sample was 10 cm. During the film deposition process, the mass deposition rate was monitored by a quartz crystal microbalance (QCM). A detailed description of the setup and the magnetrons can be found in [37–40].

The vacuum chamber was pumped down to a base pressure of 10^{-4} Pa with a turbo-molecular pump backed by a multi-stage dry Roots pump. The working gas mixtures of argon and oxygen were supplied by automated mass-flow controllers El-Flow (Bronkhorst High-Tech B.V., AK Ruurlo, The Netherlands). In all cases, the total operating pressure was fixed at 0.5 Pa. The total flow was 30 sccm. The oxygen flow range used in the experiments

was 0–3 sccm. Correspondingly, since the total gas flow was fixed at 30 sccm, the oxygen flow fraction in the Ar/O_2 gas mixture was varied from 0 to 10%. The partial pressure of oxygen was not monitored.

The magnetron was powered by a customized ELMI-600/1250S power supply (Esto-El, LLC., Zelenograd, Russia), with a maximum power of 12 kW and a maximum voltage of 1250 V. The main characteristics of the power supply are presented in Table 1.

Table 1. Parameters of the magnetron power supply.

Mode	MPPMS	HiPIMS
Pulse duration t_{on}, ms	3–30	0.03–0.3
Pause duration t_{off}, ms	100–1000	1–10
Maximum current, A	150	
Maximum voltage, V	1250	

The power supply could be operated either in MPPMS or HiPIMS mode, allowing wide room for pulse adjustment. Typical MPPMS current and voltage waveforms are shown in Figure 2.

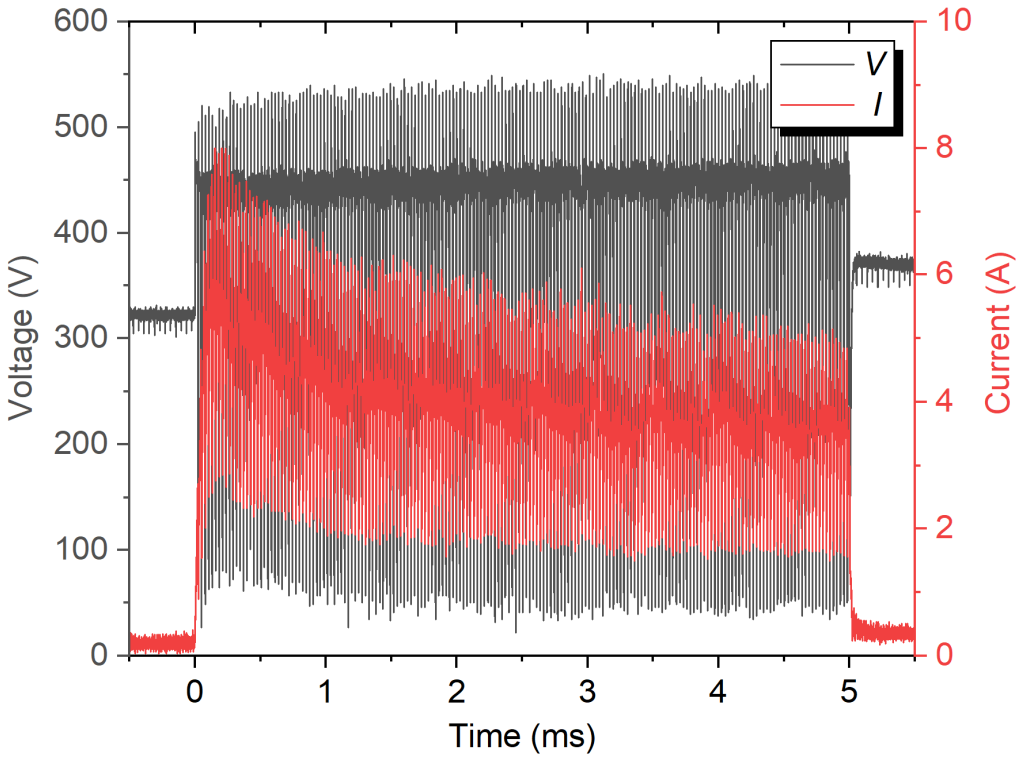

Figure 2. MPPMS discharge current and voltage waveforms (t_{on} = 5 ms).

Each individual macropulse with ms-scale pulse duration is built from short 13 µs micropulses delivered with 60 kHz repetition frequency [41]. In our case, three combinations of pulse and pause durations were used: t_{on}/t_{off} = 5 ms/100 ms, 10 ms/200 ms, and 10 ms/100 ms, so the repetition frequency was 5–10 Hz.

2.2. Sample Preparation

The coatings were deposited on glass samples 25 × 25 × 1 mm cut from the microscope slides (Thermo Scientific, Menzel Glasbearbeitungswerk GmbH & Co., Braunschweig, Germany). Prior to the experiments, they were ultrasonically washed in an alkaline cleaning solution, then in hot water, and then dried for 1 h.

2.3. Diagnostic Methods

The properties of prepared coatings were analyzed by a number of standard diagnostic methods.

2.3.1. Quartz Crystal Microbalance

QCM Mikron-5 (Izovac, LLC., Minsk, Belarus) was used to monitor the mass deposition rate during the deposition process. QCM was calibrated by experimentally determining the geometric factor, which depends on the sensor's location. Prior to the main experiments, pure aluminum films were deposited on glass substrates; their thickness was measured using a profilometer, and the deposition rate was calculated. In addition, the density of the resulting film was calculated in each case. As a result, we obtained the value of the geometric factor, which allowed the coating deposition rate to be monitored in a real-time mode. However, correct interpretation of such measurements still requires knowing the density of the deposited coating, which depends on the film composition.

2.3.2. Profilometry

A Dektak 150 (Veeco, Tucson, AZ, USA) surface profiler was used to measure the thickness and roughness of coatings deposited on glass substrates. The stylus radius was 12.5 μm, and the applied force was 10 mg.

The measurement technique involved applying a narrow strip of carbon tape to the edge of the glass substrate before the experiments, depositing a desired coating, removing the tape, and measuring the step with a profilometer.

2.3.3. Ellipsometry

The measurements were carried out on an ES-2LED installation, which is an LED spectral ellipsometer [42]. The optical properties of the samples were studied at an angle of incidence of 55 degrees for 635 nm radiation wavelength. The measurement reproducibility and stability of the ellipsometric parameters Ψ and Δ were no worse than 0.001 and 0.01°, respectively.

2.3.4. Scratch Testing

A Revetest (Anton Paar GmbH, Graz, Austria) machine was used to perform scratch testing of prepared coatings to evaluate their adhesive properties. It can apply a maximum load of 100 N in the fine range, with 0.1 mN resolution, at a scratching speed of up to 600 mm/min.

3. Results

3.1. Coating Uniformity

At first, we studied the coating thickness profile across the sample surface. In order to determine the thickness distribution of the resulting coatings, thin aluminum films were deposited on the glass substrates with initially attached masks, which covered a thin diagonal strip on each sample. After the deposition, the mask was removed, and the dependences of the coating thickness on the lateral coordinate were measured with the surface profiler. The resulting profiles are presented in Figure 3.

One can observe that the coating thickness is quite uniform over the entire sample surface. The scatter in the values is primarily due to the fact that the initial surface of the untreated glass samples was not ideally flat and had a surface roughness of Ra~20 nm.

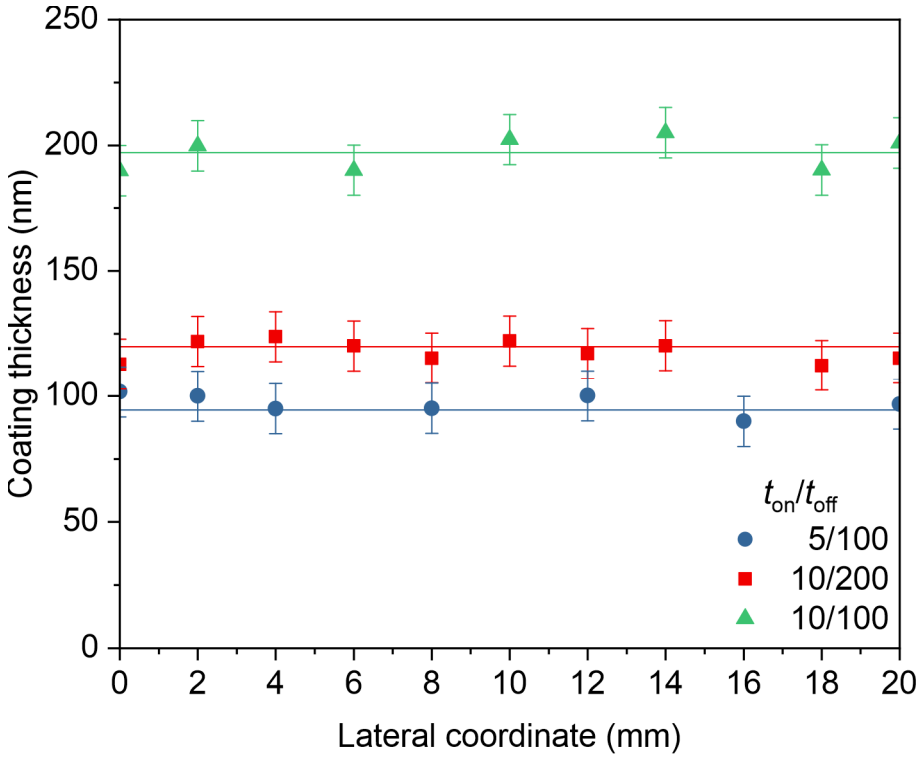

Figure 3. Dependence of coating thickness on the lateral coordinate.

3.2. Deposition Rate Measured by QCM

In order to determine the coating deposition rate, three series of experiments were carried out in three different modes: t_{on}/t_{off} = 5 ms/100 ms, 10 ms/200 ms, and 10 ms/100 ms. The discharge voltage was fixed at 500 V. In each series, the oxygen content in the vacuum chamber was changed stepwise while other parameters were kept constant. The deposition rate was measured with QCM only. As a result, the dependences of the mass deposition rate on the oxygen gas flow were obtained (Figure 4). The calculations were considering the value of the geometric factor obtained during QCM calibration.

At first, after the introduction of oxygen, the mass deposition rate increases. After that, each curve exhibits an inflection at around 0.6–0.9 sccm. The mass deposition rate reaches a plateau for t_{on}/t_{off} = 5 ms/100 ms and 10 ms/200 ms modes, while for the t_{on}/t_{off} = 10 ms/100 ms mode, it continues to grow gradually. Increasing oxygen flow above 3 sccm was associated with discharge instability due to intense target arcing. Such behavior of mass deposition rate on the oxygen flow differs from the results of [28]. Specifically, no decrease in deposition rate is observed even at the highest oxygen flow (Γ_{O2}) values. For modes with equal duty cycle values (t_{on}/t_{off} = 5 ms/100 ms and 10 ms/200 ms), the deposition rates are close to each other as expected, since the average discharge power values in these regimes are comparable.

The difference in these results from the well-known behavior of deposition rates in reactive magnetron sputtering is because of the power supply design. It should be noted that our magnetron pulsed power supply could only be operated in constant voltage mode. Therefore, neither discharge current nor power could be kept constant as the oxygen content in the gas mixture was increased. Instead, the dependence of pulsed discharge current on the oxygen flow was measured and compared for three operation modes t_{on}/t_{off} = 5 ms/100 ms, 10 ms/200 ms, and 10 ms/100 ms (Figure 5).

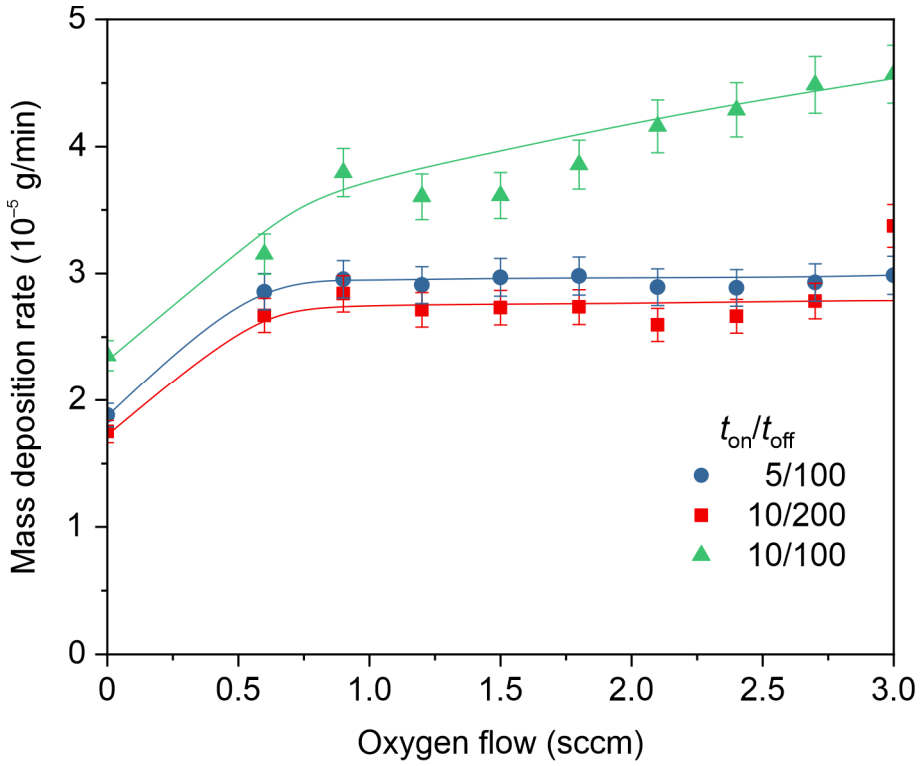

Figure 4. Dependence of the mass deposition rate on the oxygen flow.

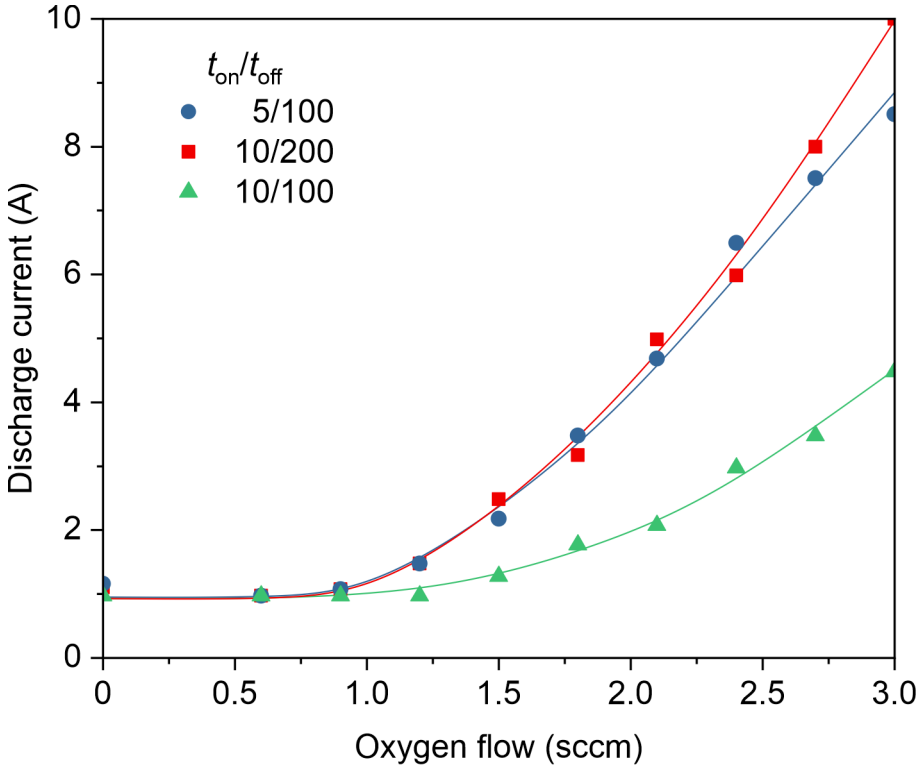

Figure 5. Dependence of the discharge current on the oxygen flow.

The current increases with increasing the oxygen flow, and its growth rate is higher in the modes with lower duty cycles, when the pulse duration is shorter or the pause duration is longer. In reactive sputtering processes, the variation of current with reactive gas flow increase is a well-known effect associated with oxide layer growth on the target surface [43].

For Al surfaces, oxidation results in enhanced ion-induced electron emission as compared to metallic Al and higher discharge current values. At the same time, sputtering of the oxide film from the target surface is more efficient for large duty cycle values, which results in a lower pulsed discharge current [41,44].

Consequently, even when keeping the same temporal parameters of the pulsing, it is incorrect to compare coating deposition rates without considering the real power applied to the target. For this reason, the rates should be normalized to the power value. Provided the voltage is constant, the mean discharge power is proportional to the pulsed discharge current and duty cycle. Therefore, with an increase in the oxygen flow, the average discharge power grows, and one would expect to observe an increase in the deposition rate. This can explain the unusual behavior of the deposition rate as a function of oxygen flow shown in Figure 4.

The discharge power was calculated from experimentally measured current and voltage values. The mass deposition rate was then divided by the mean discharge power value to yield the specific rate measured in g/min/kW, which we find more relevant for comparing different coating deposition methods. Figure 6 demonstrates the dependence of the specific deposition rate on the oxygen gas flow.

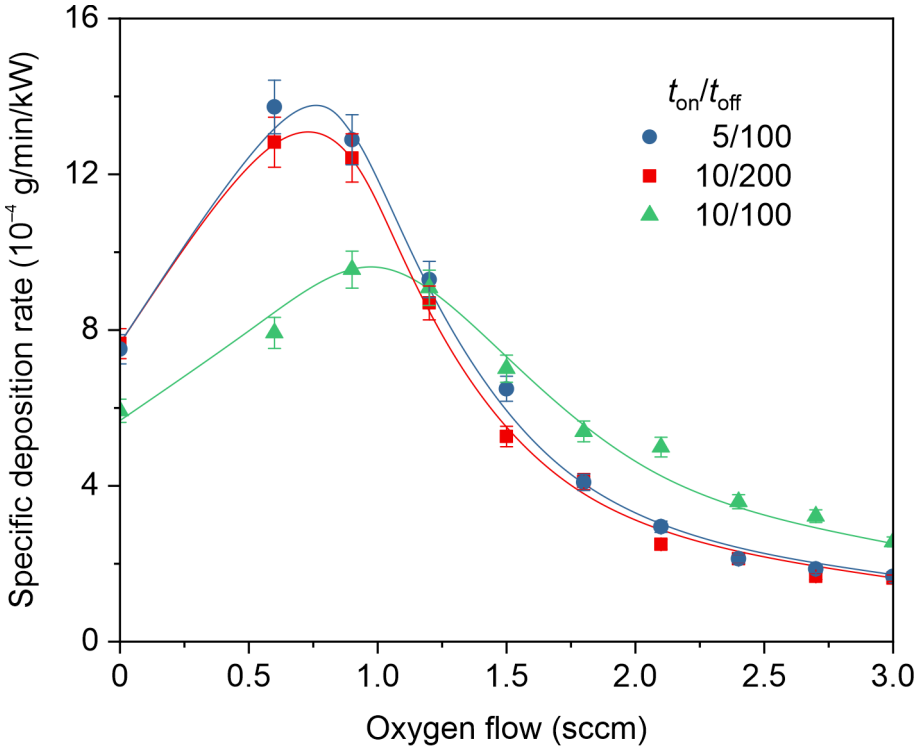

Figure 6. Dependence of the specific mass deposition rate on the oxygen gas flow.

One can notice that the resulting dependencies are now in accord with the data obtained for HiPIMS modes [28]. The decrease in the specific deposition rate starting from around a 0.6–0.9 sccm oxygen gas flow corresponds to the beginning of the transition from metallic to oxide sputtering (poisoned) mode. Consequently, we expect to obtain transparent optical coatings in the transition region, characterized by higher deposition rate values than in poisoned mode. Additionally, the gradual decrease in the deposition rate in response to the increase in oxygen flow indicates the mitigation of hysteresis effects associated with target poisoning. This is favorable for stable long-time magnetron operation without using of feedback control systems to stabilize oxygen partial pressure in the chamber.

Due to the absence of samples in this experimental series, we could assess neither the density of the applied coatings nor their optical properties. Therefore, keeping in mind the

found trends and the range of operating conditions, in the following experimental series, the aluminum oxide coatings were applied to glass substrates in the selected discharge modes.

3.3. Preparation of Aluminum Oxide Coatings

To analyze the optical and physical properties of the coatings, aluminum oxide films were deposited on glass substrates in the same three pulsing modes: t_{on}/t_{off} = 5 ms/100 ms, 10 ms/200 ms, and 10 ms/100 ms. The discharge voltage was fixed at 500 V. The main parameters of the experiment are shown in Table 2.

Table 2. List of main experimental parameters.

Sample No.	**1**	**2**	**3**	**4**	**5**	**6**	**7**	**6**	**7**	**8**	**9**	**10**	**11**	**12**	**13**
Pulse duration, ms				5						10				10	
Pause duration, ms				100						200				100	
Oxygen flow, sccm	0.60	0.75	0.90	1.20	1.50	1.65	1.80	0.75	0.90	1.05	1.20	1.50	0.90	1.20	1.50
Current, A	0.6–4														
Total pressure, Pa	0.5														
Voltage, V	500														
Duration, min	20														

Using the surface profiler, the film's thicknesses were measured, and the specific coating deposition rates were calculated. The obtained dependencies are presented in Figure 7.

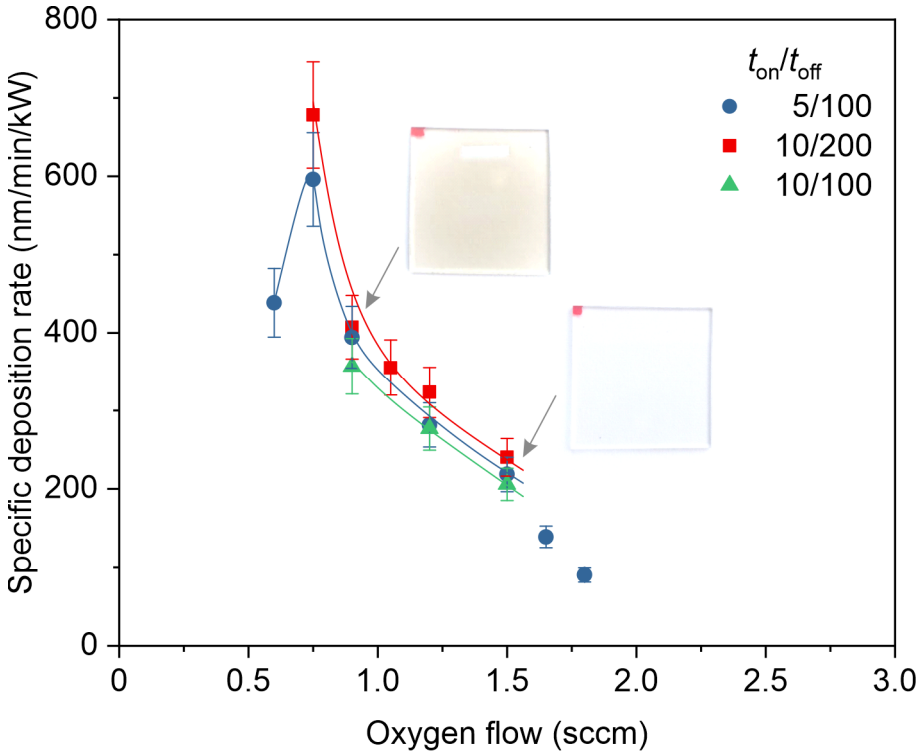

Figure 7. Dependence of specific deposition rate on the oxygen gas flow value. Photographs of samples corresponding to Γ_{O2} = 0.9 and 1.5 sccm are demonstrated.

These dependencies are consistent with similar dependencies obtained using QCM (Figure 6). As expected, the transparent coatings are grown in the transition region, which is illustrated by the inserted sample photographs. In addition, the specific deposition

rates for these samples are noticeably higher than the characteristic values for samples obtained by the HIPIMS method 70 nm/min/kW [45]. For transparent Al_2O_3 coatings, the deposition rate is 200–300 nm/min/kW, which is 50–60% of the metallic deposition rate. This means that MPPMS enables alumina coatings deposition at a faster rate than HIPIMS with the same applied power. The results are comparable with DOMS deposition aided with closed-loop feedback control of oxygen partial pressure [36], although in our case, no such control system was used, and the process was simplified to maintain a constant oxygen flow.

In most cases, after the deposition, the surface roughness of the initial sample surface was preserved and was equal to Ra ~20 nm. However, in the modes where arcing was observed on the target (the two rightmost points in Figure 7), the surface roughness was higher because of the defects introduced by macroparticle ejection from the target.

Figure 8 shows the dependences of coating density on oxygen flow for various modes obtained by measuring the mass of deposited film Δm, its thickness h, and dividing the mass over the surface area A and the thickness: $\varrho = \Delta m/(A \times h)$. The main contribution to the experimental error values originates from mass measurement uncertainty.

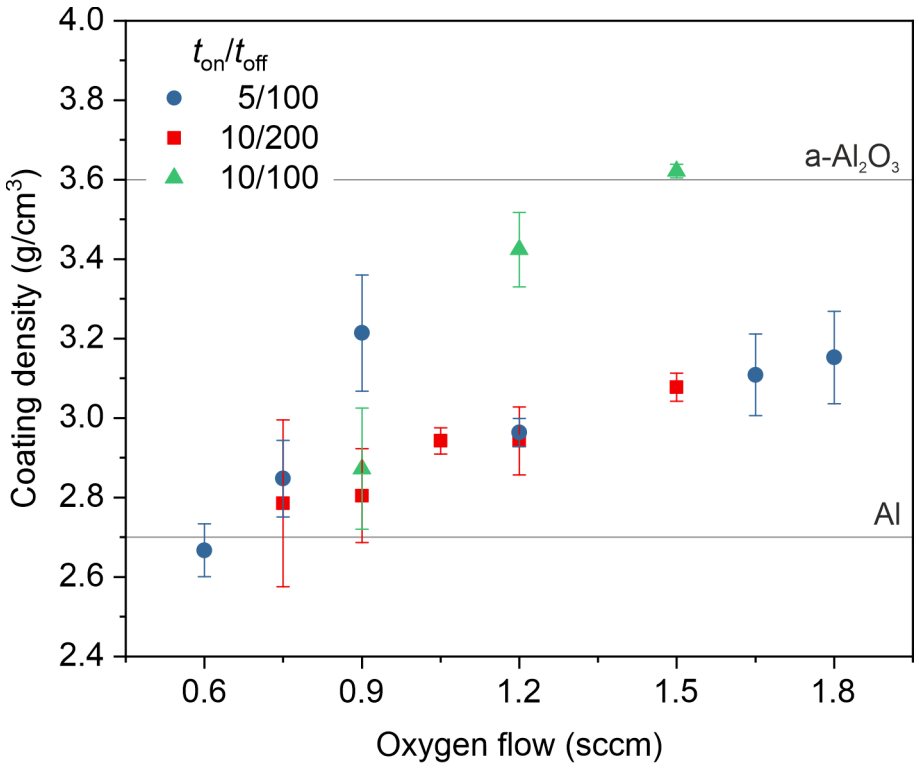

Figure 8. Dependence of coating density on oxygen flow.

The resulting aluminum oxide films have densities corresponding to the amorphous state of the oxide: 2.7–3.6 g/cm^3. One might notice that the density of coatings increases with increasing oxygen content. In this case, the growth occurs faster for the mode with a higher duty cycle (t_{on}/t_{off} = 10 ms/100 ms).

3.4. Scratch Testing

Scratch tests were performed under linearly increasing indenter load from 0.3 to 30 N at a rate of 15 N/min. The scratch length was 5 mm, and the indenter speed was 2.53 mm/min. A Rockwell diamond spherical indenter tip with 200 μm radius was used. The critical loads were detected using an acoustic sensor and visually evaluating scratch images. Figure 9 shows examples of acoustic emission and load during the scratch test and typical scratch images in characteristic regions. One can see the increase in the acoustic

signal at loads of about 4–6 N, which is associated with the cracking of deposited film. With the load increase, cracking intensifies, and the acoustic signal grows correspondingly. At the load above 7–14 N, the signal starts to fluctuate, while the images demonstrate the film's disintegration followed by the substrate's destruction.

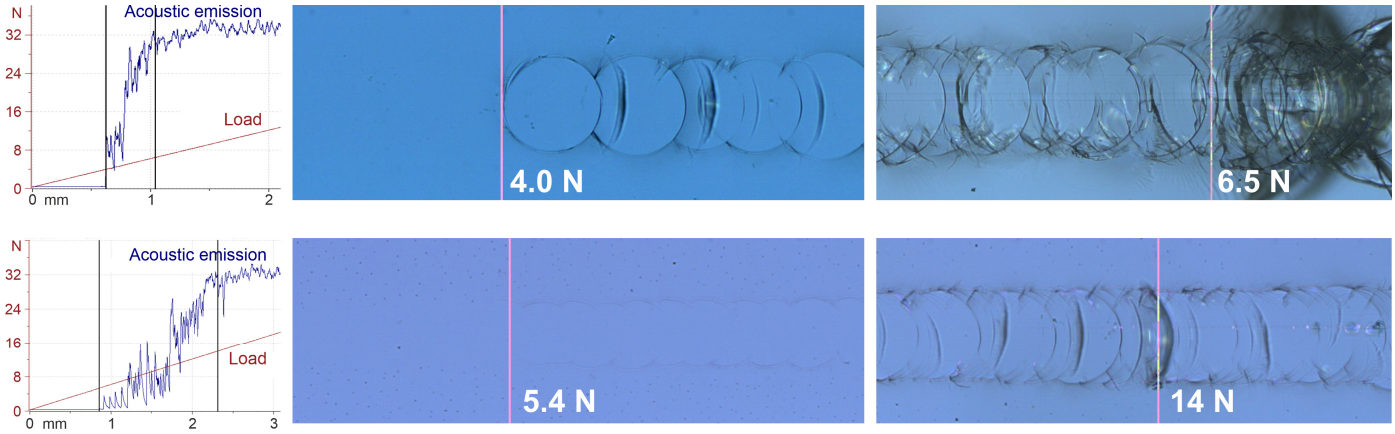

Figure 9. Scratch testing results for selected samples.

A stable acoustic emission signal after the coating fracturing corresponds to the damage of the glass substrate.

Obtained critical load values demonstrate decent adhesion of prepared coatings to the glass substrate.

3.5. Ellipsometry

The results of ellipsometry diagnostics for transparent thin films of aluminum oxide are shown in Figure 10 (extinction coefficient) and Figure 11 (refractive index).

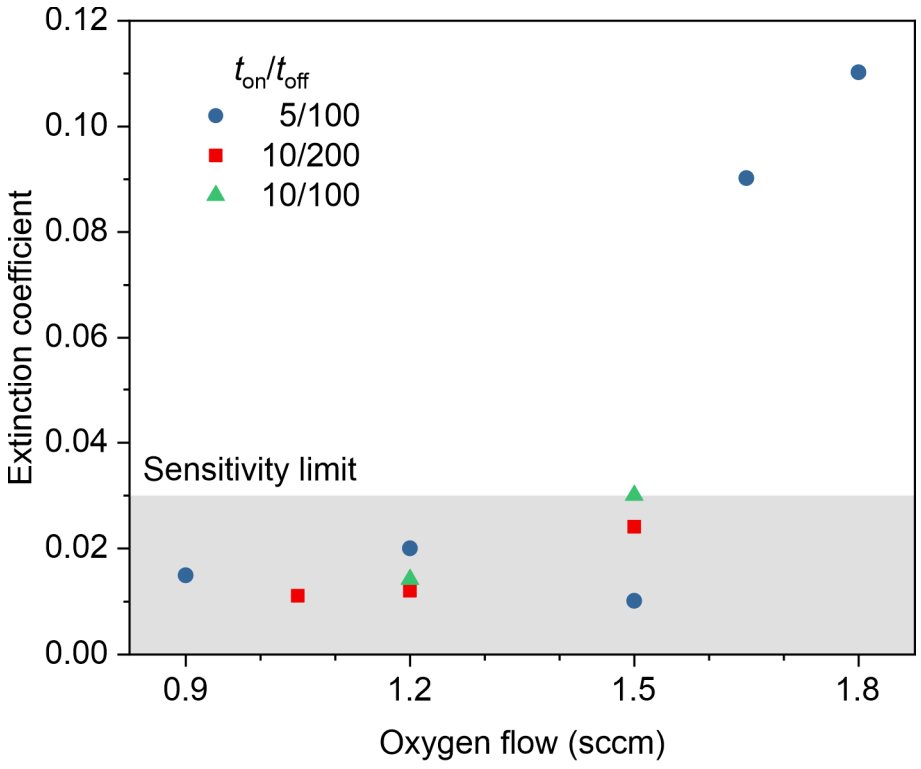

Figure 10. Dependence of extinction coefficient on oxygen content.

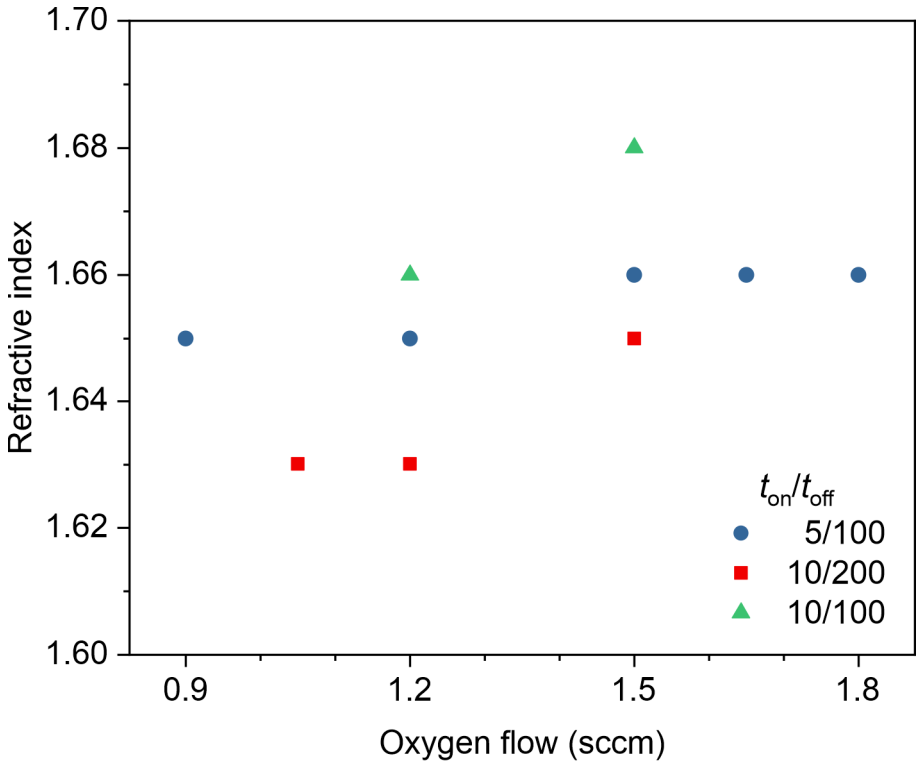

Figure 11. Dependence of refractive index on oxygen content.

Extinction coefficients for most of the samples are below the sensitivity level of the instrument used, which is 2×10^{-2}. Large absorption coefficients for samples deposited at oxygen flow values of 1.65 and 1.80 sccm can presumably be explained by the coating quality deterioration due to the microarcing on the target during the deposition process, which caused increased roughness and an abundance of surface defects.

The refractive indices for all obtained samples are higher than for samples obtained by HiPIMS (n = 1.60) [29].

4. Discussion

The different pulse lengths can explain the difference in the parameters of coatings obtained in MPPMS and HiPIMS. In pulsed magnetron sputtering systems, the flux of sputtered atoms onto the substrate is modulated in accordance with the pulsing regime [46]. In addition, the amplitude of the flux modulation depends on other factors; however, in some cases it can be neglected. A sketch of the dynamics of sputtering and deposition fluxes of target species with a pack of five pulses is presented in Figure 12. As the pause between pulses increases, the modulation of the atomic flux increases and, as a result, the flux onto the substrate becomes essentially nonuniform in time. With a triangular shape of current pulses, which is usually the case for HiPIMS modes [47], the flux modulation would be even more pronounced than with a rectangular shape.

In the case of MPPMS, the pulse length is longer than the characteristic deposition time of aluminum atoms. Therefore, the flux onto the substrate during the pulse is relatively uniform, and as a result, the parameters of the coatings are improved.

In the HiPIMS case, short pulses are used, with their shape different from rectangular and more similar to the triangular one. Consequently, the flux of sputtered metal atoms onto the substrate becomes inhomogeneous over time and the coating quality might deteriorate.

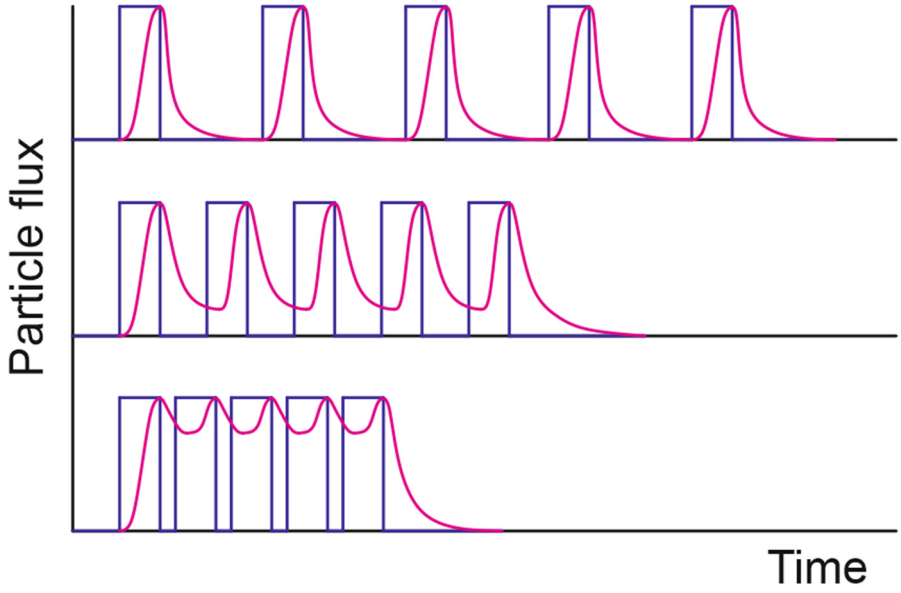

Figure 12. A sketch of the dynamics of sputtering pulses (blue curves) and deposition flux (magenta curves) of atoms in MPPMS mode with a rectangular shape of current pulses.

Moreover, apart from the modulation of atomic fluxes, the shape of discharge pulses and pulsing mode affect the reactive deposition outcome. This is because the stability of the reactive sputtering process is sensitive to the characteristic times of sputtering and oxidizing stages [24,36]. The thickness of the insulating layer that is grown on the target surface and is responsible for the arcing exhibits variations associated with the form of discharge current pulses. If the pulses are short and have a large magnitude, the arcing events occur frequently, with a pronounced negative effect on coating properties.

One of the approaches for improving the HiPIMS performance in this case is to combine it with mid-frequency pulsed DC sputtering [24]. However, it requires using at least two power supplies and properly syncing between their output signals. As the DOMS modes, the HiPIMS+MF ones imply using a feedback loop control system for oxygen pressure to ensure high productivity of the deposition process. Therefore, the ability to prepare transparent alumina coatings at high deposition rates without using such control systems and with a single power supply is an advantage, making the studied MPPMS modes both energy- and cost-effective, at least for producing alumina oxide coatings.

5. Conclusions

The specific deposition rate of 200 nm/min/kW was obtained in MPPMS modes with ms-scale pulses for the preparation of highly transparent Al_2O_3 films with densities up to 3.6 g/cm^3, characteristic of amorphous Al_2O_3, which makes MPPMS superior to short-pulse HiPIMS modes. The refractive indices for all MPPMS-deposited coatings (n = 1.63–1.68) are higher than those reported for the short-pulse HiPIMS method (n = 1.60) without substrate heating. The density and the refractive index are higher for the coatings prepared with a higher duty factor. For all samples, the extinction coefficient is below the instrument sensitivity level ($k < 10^{-2}$).

The lack of need to utilize an oxygen pressure feedback loop to maintain a stable and highly productive deposition process is an advantage, making the discussed MPPMS modes both energy- and cost-effective, at least for producing alumina oxide coatings.

Author Contributions: Conceptualization, A.V.T.; Data curation, D.V.K., M.M.K. and K.Y.O.; Funding acquisition, N.N.S.; Investigation, A.V.T., M.M.K. and T.V.S.; Methodology, D.V.K.; Project administration, A.V.K. and N.N.S.; Software, D.V.K. and K.Y.O.; Supervision, A.V.K.; Visualization, T.V.S.; Writing—original draft, A.V.K.; Writing—review and editing, N.N.S. All authors have read and agreed to the published version of the manuscript.

Funding: This work was carried out within the framework of the state task of the Ministry of Science and Higher Education of the Russian Federation (subject No. FSWU-2022-0022 "Low-temperature ceramic technologies (LTCC) in microelectronics").

Institutional Review Board Statement: Not applicable.

Informed Consent Statement: Not applicable.

Data Availability Statement: The data presented in this study are available on request from the corresponding author.

Conflicts of Interest: The authors declare no conflicts of interest. The funders had no role in the design of the study; in the collection, analyses, or interpretation of data; in the writing of the manuscript; or in the decision to publish the results.

References

1. Hu, B.; Yao, M.; Xiao, R.; Chen, J.; Yao, X. Optical Properties of Amorphous Al_2O_3 Thin Films Prepared by a Sol–Gel Process. *Ceram. Int.* **2014**, *40*, 14133–14139. [CrossRef]
2. Schubert, E.F.; Passlack, M.; Hong, M.; Mannerts, J.; Opila, R.L.; Pfeiffer, L.N.; West, K.W.; Bethea, C.G.; Zydzik, G.J. Properties of Al_2O_3 Optical Coatings on GaAs Produced by Oxidation of Epitaxial AlAs/GaAs Films. *Appl. Phys. Lett.* **1994**, *64*, 2976–2978. [CrossRef]
3. Korhonen, H.; Syväluoto, A.; Leskinen, J.T.T.; Lappalainen, R. Optically Transparent and Durable Al_2O_3 Coatings for Harsh Environments by Ultra Short Pulsed Laser Deposition. *Opt. Laser Technol.* **2018**, *98*, 373–384. [CrossRef]
4. Niu, D.; Wang, Q.; Zhang, C.; Cheng, P.; Wang, Y.; Zhang, J.; Ding, G.; Xie, K.; Shao, J.; Liu, Y.; et al. Preparation, Characterization and Application of High-Temperature Al_2O_3 Insulating Film. *Surf. Coat. Technol.* **2016**, *291*, 318–324. [CrossRef]
5. Bartzsch, H.; Glöß, D.; Böcher, B.; Frach, P.; Goedicke, K. Properties of SiO_2 and Al_2O_3 Films for Electrical Insulation Applications Deposited by Reactive Pulse Magnetron Sputtering. *Surf. Coat. Technol.* **2003**, *174–175*, 774–778. [CrossRef]
6. Edlmayr, V.; Moser, M.; Walter, C.; Mitterer, C. Thermal Stability of Sputtered Al_2O_3 Coatings. *Surf. Coat. Technol.* **2010**, *204*, 1576–1581. [CrossRef]
7. García Ferré, F.; Ormellese, M.; Di Fonzo, F.; Beghi, M.G. Advanced Al_2O_3 Coatings for High Temperature Operation of Steels in Heavy Liquid Metals: A Preliminary Study. *Corros. Sci.* **2013**, *77*, 375–378. [CrossRef]
8. Ruppi, S.; Larsson, A.; Flink, A. Nanoindentation Hardness, Texture and Microstructure of α-Al_2O_3 and κ-Al_2O_3 Coatings. *Thin Solid Films* **2008**, *516*, 5959–5966. [CrossRef]
9. Yu, Y.; Zuo, Y.; Zhang, Z.; Wu, L.; Ning, C.; Zuo, C. Al_2O_3 Coatings on Zinc for Anti-Corrosion in Alkaline Solution by Electrospinning. *Coatings* **2019**, *9*, 692. [CrossRef]
10. Liu, C.; Wang, W.; Yang, T.; Liu, Y.; Tang, Z.; Liu, W.; Liu, S. Effect of High-Temperature Thermal Shock on Solar Absorption Rate of Alumina Coating. *Coatings* **2023**, *13*, 1527. [CrossRef]
11. Yin, X.; Wang, Y.; Wang, H.; Zhao, K.; Sun, Y.; Xiao, J.; Zhao, Y.; Gong, F.; Chen, Y. Corrosion Behavior and Failure Mechanism of Amorphous Al_2O_3 Coating at High-Temperature LBE. *Vacuum* **2023**, *215*, 112251. [CrossRef]
12. Khanna, A.; Bhat, D.G. Nanocrystalline Gamma Alumina Coatings by Inverted Cylindrical Magnetron Sputtering. *Surf. Coat. Technol.* **2006**, *201*, 168–173. [CrossRef]
13. Choy, K. Chemical Vapour Deposition of Coatings. *Prog. Mater. Sci.* **2003**, *48*, 57–170. [CrossRef]
14. Vereschaka, A.; Milovich, F.; Andreev, N.; Sotova, C.; Alexandrov, I.; Muranov, A.; Mikhailov, M.; Tatarkanov, A. Investigation of the Structure and Phase Composition of the Microdroplets Formed during the Deposition of PVD Coatings. *Surf. Coat. Technol.* **2022**, *441*, 128574. [CrossRef]
15. Safi, I. Recent Aspects Concerning DC Reactive Magnetron Sputtering of Thin Films: A Review. *Surf. Coat. Technol.* **2000**, *127*, 203–218. [CrossRef]
16. Musil, J.; Baroch, P.; Vlček, J.; Nam, K.H.; Han, J.G. Reactive Magnetron Sputtering of Thin Films: Present Status and Trends. *Thin Solid Films* **2005**, *475*, 208–218. [CrossRef]
17. Cheng, Y.; Qiu, W.; Zhou, K.; Yang, Y.; Jiao, D.; Liu, Z.; Zhong, X. Low-Temperature Deposition of α-Al_2O_3 Film Using Al+α-Al_2O_3 Composite Target by Radio Frequency Magnetron Sputtering. *Mater. Res. Express* **2019**, *6*, 086412. [CrossRef]
18. Strijckmans, K.; Schelfhout, R.; Depla, D. Tutorial: Hysteresis during the Reactive Magnetron Sputtering Process. *J. Appl. Phys.* **2018**, *124*, 241101. [CrossRef]
19. Gudmundsson, J.T. Physics and Technology of Magnetron Sputtering Discharges. *Plasma Sources Sci. Technol.* **2020**, *29*, 113001. [CrossRef]
20. Strijckmans, K.; Moens, F.; Depla, D. Perspective: Is There a Hysteresis during Reactive High Power Impulse Magnetron Sputtering (R-HiPIMS)? *J. Appl. Phys.* **2017**, *121*, 080901. [CrossRef]
21. Sarakinos, K.; Alami, J.; Wuttig, M. Process Characteristics and Film Properties upon Growth of TiOx Films by High Power Pulsed Magnetron Sputtering. *J. Phys. D Appl. Phys.* **2007**, *40*, 2108–2114. [CrossRef]

22. Sarakinos, K.; Alami, J.; Klever, C.; Wuttig, M. Process Stabilization and Enhancement of Deposition Rate during Reactive High Power Pulsed Magnetron Sputtering of Zirconium Oxide. *Surf. Coat. Technol.* **2008**, *202*, 5033–5035. [CrossRef]
23. Čapek, J.; Kadlec, S. Return of Target Material Ions Leads to a Reduced Hysteresis in Reactive High Power Impulse Magnetron Sputtering: Experiment. *J. Appl. Phys.* **2017**, *121*, 171911. [CrossRef]
24. Ferreira, M.P.; Martínez-Martínez, D.; Chemin, J.-B.; Choquet, P. Tuning the Characteristics of Al_2O_3 Thin Films Using Different Pulse Configurations: Mid-Frequency, High-Power Impulse Magnetron Sputtering, and Their Combination. *Surf. Coat. Technol.* **2023**, *466*, 129648. [CrossRef]
25. Mareš, P.; Dubau, M.; Polášek, J.; Mates, T.; Kozák, T.; Vyskočil, J. High Deposition Rate Films Prepared by Reactive HiPIMS. *Vacuum* **2021**, *191*, 110329. [CrossRef]
26. Kagerer, S.; Zauner, L.; Wojcik, T.; Kolozsvári, S.; Kozák, T.; Čapek, J.; Zeman, P.; Riedl, H.; Mayrhofer, P.H. Reactive HiPIMS Deposition of Al-Oxide Thin Films Using W-Alloyed Al Targets. *Surf. Coat. Technol.* **2021**, *422*, 127467. [CrossRef]
27. Sproul, W.D.; Lin, J.; Moore, J.J.; Wu, Z.; Zhang, X.; Chistyakov, R.; Abraham, B.; Rees, A. Mass/Energy Analysis of a Modulated Pulse Power Plasma Compared to a DC Plasma. In Proceedings of the 52nd SVC Technical Conference, Santa Clara, CA, USA, 9–14 May 2009.
28. Wallin, E.; Helmersson, U. Hysteresis-Free Reactive High Power Impulse Magnetron Sputtering. *Thin Solid Films* **2008**, *516*, 6398–6401. [CrossRef]
29. Houska, J.; Blazek, J.; Rezek, J.; Proksova, S. Overview of Optical Properties of Al_2O_3 Films Prepared by Various Techniques. *Thin Solid Films* **2012**, *520*, 5405–5408. [CrossRef]
30. Diyatmika, W.; Liang, F.-K.; Lou, B.-S.; Lu, J.-H.; Sun, D.-E.; Lee, J.-W. Superimposed High Power Impulse and Middle Frequency Magnetron Sputtering: Role of Pulse Duration and Average Power of Middle Frequency. *Surf. Coat. Technol.* **2018**, *352*, 680–689. [CrossRef]
31. Moirangthem, I.; Chen, S.-H.; Lou, B.-S.; Lee, J.-W. Microstructural, Mechanical and Optical Properties of Tungsten Oxide Coatings Fabricated Using Superimposed HiPIMS-MF Systems. *Surf. Coat. Technol.* **2022**, *436*, 128314. [CrossRef]
32. Olejníček, J.; Hubička, Z.; Kment, Š.; Čada, M.; Kšírová, P.; Adámek, P.; Gregora, I. Investigation of Reactive HiPIMS+MF Sputtering of TiO_2 Crystalline Thin Films. *Surf. Coat. Technol.* **2013**, *232*, 376–383. [CrossRef]
33. Lin, J.; Moore, J.J.; Sproul, W.D.; Lee, S.L. Effects of the Magnetic Field Strength on the Modulated Pulsed Power Magnetron Sputtering of Metallic Films. *J. Vac. Sci. Technol. A Vac. Surf. Films* **2011**, *29*, 061301. [CrossRef]
34. Lin, J.; Moore, J.J.; Sproul, W.D.; Mishra, B.; Wu, Z.; Wang, J. The Structure and Properties of Chromium Nitride Coatings Deposited Using Dc, Pulsed Dc and Modulated Pulse Power Magnetron Sputtering. *Surf. Coat. Technol.* **2010**, *204*, 2230–2239. [CrossRef]
35. Lin, J.; Sproul, W.D.; Moore, J.J.; Lee, S.; Myers, S. High Rate Deposition of Thick CrN and Cr_2N Coatings Using Modulated Pulse Power (MPP) Magnetron Sputtering. *Surf. Coat. Technol.* **2011**, *205*, 3226–3234. [CrossRef]
36. Lin, J. High Rate Reactive Sputtering of Al_2O_3 Coatings by HiPIMS. *Surf. Coat. Technol.* **2019**, *357*, 402–411. [CrossRef]
37. Kaziev, A.V.; Kolodko, D.V.; Lisenkov, V.Y.; Tumarkin, A.V.; Kharkov, M.M.; Samotaev, N.N.; Oblov, K.Y. Cu Metallization of Al_2O_3Ceramic by Coating Deposition from Cooled- and Hot-Target Magnetrons. *Coatings* **2023**, *13*, 238. [CrossRef]
38. Kaziev, A.V.; Ageychenkov, D.G.; Tumarkin, A.V.; Kolodko, D.V.; Sergeev, N.S.; Kharkov, M.M.; Leonova, K.A. Ion Current Optimization in a Magnetron with Tunable Magnetic Field Configuration. *J. Phys. Conf. Ser.* **2021**, *2064*, 012061. [CrossRef]
39. Ageychenkov, D.G.; Kaziev, A.V.; Kolodko, D.V.; Isakova, A.S. Layer-by-Layer Deposition of Transparent AZO Coatings on Polymer Surfaces in a DC Magnetron Discharge. In Proceedings of the 8th International Congress on Energy Fluxes and Radiation Effects, Tomsk, Russia, 2–8 October 2022; pp. 1032–1035. [CrossRef]
40. Burmistrov, D.E.; Yanykin, D.V.; Paskhin, M.O.; Nagaev, E.V.; Efimov, A.D.; Kaziev, A.V.; Ageychenkov, D.G.; Gudkov, S.V. Additive Production of a Material Based on an Acrylic Polymer with a Nanoscale Layer of Zno Nanorods Deposited Using a Direct Current Magnetron Discharge: Morphology, Photoconversion Properties, and Biosafety. *Materials* **2021**, *14*, 6586. [CrossRef]
41. Kaziev, A.V.; Kolodko, D.V.; Sergeev, N.S. Properties of Millisecond-Scale Modulated Pulsed Power Magnetron Discharge Applied for Reactive Sputtering of Zirconia. *Plasma Sources Sci. Technol.* **2021**, *30*, 055002. [CrossRef]
42. Kovalev, V.I.; Rukovishnikov, A.I.; Kovalev, S.V.; Kovalev, V.V. LED Broadband Spectral Ellipsometer with Switching of Orthogonal Polarization States. *J. Opt. Technol.* **2016**, *83*, 181–184. [CrossRef]
43. Aiempanakit, M.; Aijaz, A.; Lundin, D.; Helmersson, U.; Kubart, T. Understanding the Discharge Current Behavior in Reactive High Power Impulse Magnetron Sputtering of Oxides. *J. Appl. Phys.* **2013**, *113*, 133302. [CrossRef]
44. Hippler, R.; Cada, M.; Mutzke, A.; Hubicka, Z. Pulse Length Dependence of a Reactive High Power Impulse Magnetron (HiPIMS) Discharge. *Plasma Sources Sci. Technol.* **2023**, *32*, 055013. [CrossRef]
45. Kohout, J.; Bousser, E.; Schmitt, T.; Vernhes, R.; Zabeida, O.; Klemberg-Sapieha, J.; Martinu, L. Stable Reactive Deposition of Amorphous Al_2O_3 Films with Low Residual Stress and Enhanced Toughness Using Pulsed Dc Magnetron Sputtering with Very Low Duty Cycle. *Vacuum* **2016**, *124*, 96–100. [CrossRef]

46. Greczynski, G.; Petrov, I.; Greene, J.E.; Hultman, L. Paradigm Shift in Thin-Film Growth by Magnetron Sputtering: From Gas-Ion to Metal-Ion Irradiation of the Growing Film. *J. Vac. Sci. Technol. A Vac. Surf. Films* **2019**, *37*, 060801. [CrossRef]
47. Layes, V.; Corbella, C.; Monjé, S.; Schulz-Von Der Gathen, V.; Von Keudell, A.; De Los Arcos, T. Connection between Target Poisoning and Current Waveforms in Reactive High-Power Impulse Magnetron Sputtering of Chromium. *Plasma Sources Sci. Technol.* **2018**, *27*, 084004. [CrossRef]